**Geomechanics and Engineering**, *Vol. 15, No. 5 (2018) 1101-1111*
DOI: https://doi.org/10.12989/gae.2018.15.5.1101


# Static behavior of a laterally loaded guardrail post in sloping ground by LS-DYNA

Kwang S. Woo[1], Dong W. Lee[2], Seung H. Yang[1] and Jae S. Ahn[*3]

[1]*Department of Civil Engineering, Yeungnam University, 280 Daehak-Ro, Gyeongsan, Gyeongbuk 38541, Republic of Korea*
[2]*Soohyung Industry Development Co. Ltd. 47-16 Gongdan-ro 11-gil, Waegwan-eup, Chilgok-gun, Gyeongbuk 39910, Republic of Korea*
[3]*School of General Education, Yeungnam University, 280 Daehak-Ro, Gyeongsan, Gyeongbuk 38541, Republic of Korea*

*(Received February 7, 2017, Revised January 26, 2018, Accepted February 19, 2018)*

**Abstract.** This study aims to present accurate soil modeling and validation of a single roadside guardrail post as well as a single concrete pile installed near cut slopes or compacted sloping embankment. The conventional Winkler's elastic spring model and p-y curve approach for horizontal ground cannot directly be applied to sloping ground where ultimate soil resistance is significantly dependent on ground inclination. In this study, both grid-based 3-D FE model and particle-based SPH (smoothed particle hydrodynamics) model available in LS-DYNA have been adopted to predict the static behavior of a laterally loaded guardrail post. The SPH model has potential to eliminate any artificial soil stiffness due to the deterioration of the node-connected Lagrangian soil mesh. For this purpose, this study comprises two parts. Firstly, only 3-D FE modeling has been tested to show the numerical validity for a single concrete pile in sloping ground using Mohr-Coulomb material. However, this material option cannot be implemented for SPH elements. Nevertheless, Mohr-Coulomb model has been used since this material model requires six input soil data that can be obtained from the comparative papers in literatures. Secondly, this work is extended to compute the lateral resistance of a guardrail post located near the slope using the hybrid approach that combines Lagrange FE elements and SPH elements by the suitable node-merging option provided by LS-DYNA. For this analysis, the FHWA soil material developed for application to road-base soils has been used and also allows the application of SPH element.

**Keywords:** finite element method; nonlinearity; numerical analyses; soil modeling; soil-structure interaction

## 1. Introduction

The roadside guardrail systems generally comprise three parts such as guardrail beams, distance spacers and guardrail posts as shown in Fig. 1. The lateral behavior of guardrail posts can be somewhat different from concrete or steel piles. The length and dimension of guardrail posts are very small scale as compared with conventional piles totally embedded in soils. Also, the guardrail post partly embedded in soils can be subjected to bending moment due to lateral load applied at the certain point of overhang from the ground level. This deformable guardrail posts are exposed to considerable lateral loads during the vehicle collision. In many practical situations, guardrail posts in a roadway can be installed on cut slopes or compacted sloping embankment. Thus the suitable soil modeling considering ground inclination is needed according to different soil material characteristics. Plaxico *et al*. (1998) evaluated the performance of many guardrail terminal systems considering the strength of timber guardrail posts and soil conditions. The MGS(Midwest Guardrail System: 31" tall W-beam guardrail) with an omitted post was evaluated by Lingenfelter *et al*. (2016) according to the safety performance criteria provided in MASH. Following the full-scale crash testing, implementation guidance and recommendations were provided regarding omission of a post within various MGS configurations, including MGS adjacent to 2:1 fill slopes, MGS on 8:1 approach slopes, MGS in combination with curbs, etc.

However, unfortunately, there are a few research papers (Wu and Thomson 2007, Sheikh *et al*. 2011) regarding static or dynamic performance of a single guardrail post by the finite element approaches that are also limited to the horizontal ground only as shown in Fig.2. The finite element model considering ground inclination has been attempted for the vehicle impact analysis of W-beam guardrail system with different post shapes by Lee *et al*. (2014). However, the numerical results by Lee *et al*. (2014) give a motivation to extend this work to investigate the static and dynamic performance of a single guardrail post near slopes for enhancement of numerical accuracy of the crash test of guardrail system. Unlike roadside guardrail posts, a lot of research papers on the pile analysis not only for horizontal but also sloping ground in the area of foundation engineering as described below. Thus this paper consists of two parts. To validate numerical models, the static behavior of a laterally loaded single concrete pile has been tested in the first part since no helpful experimental or numerical results are detected from the literature reviews related to a single guardrail post. Therefore, we will deal with the lateral resistance of a single guardrail post in the second part.

Although evaluation of soil-structure interface has been

∗Corresponding author, Professor
E-mail: jsahn@ynu.ac.kr


http://www.techno-press.org/?journal=gae&subpage=7
ISSN: 2005-307X (Print), 2092-6219 (Online)

extensively studied by experiments (Cabalar 2016) and numerical techniques (Jafarnia and Varzaghani 2016) , it is still difficult to predict rational results dependent on many factors as normal stresses, surface roughness, particle, dilation angles of soils etc. (Zhang *et al*. 2016). As you aware of it, in the past works of pile analyses, the response of piles to lateral loads has usually been analyzed by the well-known subgrade reaction technique, where the pile is considered as an elastic beam supported by either a Winkler's elastic spring or a series of nonlinear springs (Hirai 2012). There are a lot of research papers concerning to the use of this method to determine the appropriate lateral load-displacement relationships (*p-y* curves) for horizontal ground using the nonlinear spring model. The available *p-y* curve for horizontal ground cannot be directly applied to sloping ground, since the ground inclination significantly affects the ultimate soil resistance close to the ground surface (Chae *et al*. 2004). Thus the 3-D finite element model is one of realistic alternatives to predict the load-deflection behavior of laterally loaded structures in sloping ground. However, a point at issue seems to be the finite element modeling of the interfaces between the pile and soil. It has been argued that the conventional Lagrangian finite element modeling may result in an artificially high resistance, due to the increasing distortion of the soil mesh as the movement of the pile in the soil becomes large (Sheikh *et al*. 2009). This is because most of the previous works are based on the node-connected Lagrangian finite element models. Some researchers have tried to use special interface elements to handle this problem. For instance, Georgiadis and Georgiadis (2010) used a linear elastic-perfectly plastic Tresca material model for soil using the PLAXIS 3D Foundation V2.2 program. A thin zone of 0.1*D* (*D* = diameter of pile) around the pile was assigned with zero tensile strength, in order to allow effective soil-pile separation at the back of the pile. To the best of our knowledge, however, this is a temporary expedient. Thus, ideally, we need to find a way to separate the soil from the pile using a suitable interface modeling based on the contact element concept. One strategy in LS-DYNA is to use the CONTACT_SURFACE _TO_SURFACE option considering a friction coefficient at the separated interface. It is also expected that the SPH (smoothed particle hydrodynamics) element based on the concept of the particle method would eliminate any artificial soil stiffness resulting from the deterioration of the Lagrangian soil mesh. In applied mechanics, the SPH method is considered to be powerful and useful for those problems that involve large displacements (Sheikh *et al*. 2009, Nastasescu 2010). To combine the grid-based 3-D finite elements with the particle-based SPH elements at the interface, CONTACT_TIED_ NODES _TO_SURFACE option has been used.

The aim of this study is to validate the grid-based 3-D finite element model as well as the particle-based SPH model for a laterally loaded guardrail post embedded in sloping ground with the help of two numerical examples. The first example is the evaluation of the lateral resistance of a single concrete pile using the 3-D finite element model associated with Mohr-Coulomb soil material model. The *p-y* curve represents the relationship between the lateral load

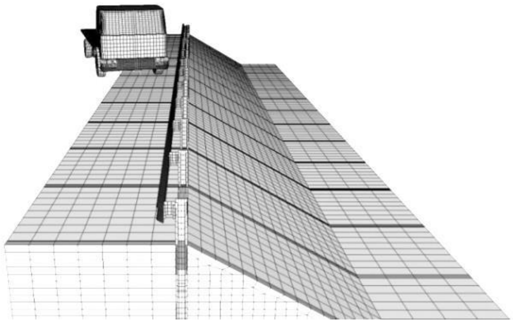

(a) Guardrail system

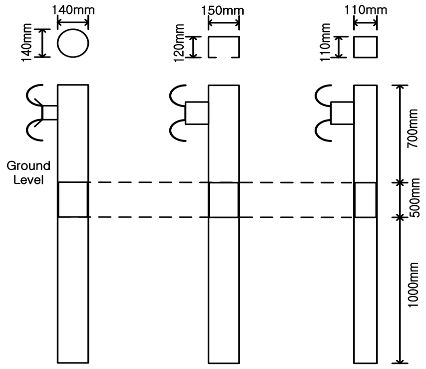


(b) Guardrail post

Fig. 1 FE model for W-beam guardrail system in sloping ground (Lee 2014)

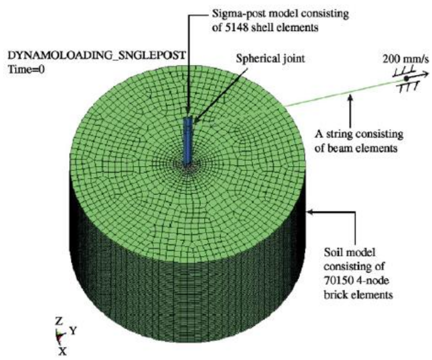


(a) Model of a single post in soil (Wu and Thomson 2007)

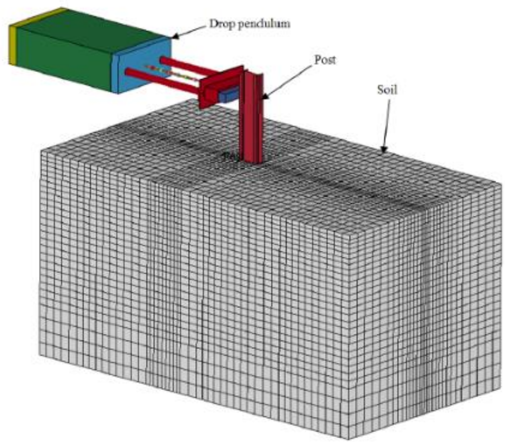


(b) Model of pendulum impact post in soil (Sheikh *et al.* 2011)

Fig. 2 The soil model for a laterally loaded guardrail post in horizontal ground per unit pile length ($p$) and the lateral displacement ($y$) at a given point in the pile. In the second example, the hybrid model combining 3-D FE elements with SPH elements using FHWA road-based soil material model is employed to evaluate the effect of ground inclination and ultimate lateral resistance of a guardrail post. For this purpose, HYPER-MESH and LS-DYNA (LSTC, 2012) programs have been used for modeling and running.

## 2. *p-y* curve estimation for sloping ground

The *p-y* approach (Matlock 1970, Reese *et al.* 1974, Reese and Welch 1975) is originated from the subgrade reaction method representing a relationship between lateral load per unit length $p$ and deflection $y$ of pile along the pile length. This curve generally shows a nonlinear behavior, thus Matlock (1970), Reese *et al.* (1974), and Reese and Welch (1975) proposed the empirical equation to represent the *p-y* curve using a power function for the analysis of laterally loaded piles in undrained soils.

$$p = 0.5p_u(y/y_c)^{\beta} \tag{1}$$

where $p_u$ is the ultimate load (load per unit pile length), $y_c$ the reference displacement at 50 % of $p_u$ and $\beta$ the empirical coefficient. However, this equation shows a very small deflection at the low horizontal load since the initial tangent to *p-y* curve denoted by $K_i$ causes a considerable high gradient of curve slope. Thus, the hyperbolic function considering an initial slope Ki in Eq. (2) was presented by Kim et al. (2004), and Georgiadis and Georgiadis (2010) as a *p-y* curve for sand.

$$p = \frac{y}{(1/K_i) + (y/p_u)} \tag{2}$$

In order to compute the ultimate $p_u$ near the ground surface, Matlock (1970) provided a suitable equation based on the flow-around failure theory as follows;

$$p_u = N_p C_u D \tag{3}$$

where $C_u$ and $D$ are the undrained shear strength at depth $z$ and the diameter of a drilled shaft. Also, $N_p$ means the lateral bearing capacity factor varying from an initial value $N_{po}$ to a maximum value $N_{pu}$ along the depth z. For sloping ground, the lateral bearing capacity factor $N_p$ should include the slope of ground $\theta$. For this purpose, Murff and Hamilton (1993) suggested the following equation.

$$N_p = N_{pu} - \left(N_{pu} - N_{po}\cos\theta\right)e^{-\lambda(z/D)/(1+\tan\theta)} \tag{4}$$

where $\lambda$ is a non-dimensional factor that varies with the soil-pile adhesion factor that varies linearly from 0.4 to 0.55 by Georgiadis and Georgiadis (2010). Several investigators have worked on the initial stiffness $K_i$ of the *p-y* curve. Firstly, Vesic (1961) presented an elastic solution based on Winkler's hypothesis and Carter (1984) modified from Vesic's equation (Vesic 1961) to find a non-linear soil model for prediction lateral pile response considering the effect of pile diameter. In this study, however, the initial stiffness $K_i$ in Eq. (5) has been adopted to compare the numerical solutions obtained by present FEM modeling with the reference value as a theoretical solution proposed by Georgiadis and Georgiadis (2010) as follows

$$K_i = 3E_{50}\left(\frac{E_{50}D^4}{E_p I_p}\right)^{1/12} \tag{5}$$

## 3. Soil material models in LS-DYNA

### *3.1 MAT173: Mohr- Coulomb model*

This material model, introduced in LS-DYNA (LSTC 2012), provides a linear shear failure surface, based on the well-known Mohr-Coulomb model for the pressure dependent shear strength (Jiang 2011).

$$\tau = \mathrm{c} + p\tan\varphi \tag{6}$$

where $c$ and $\varphi$ represent the cohesion and friction angle values of the Mohr-Coulomb yield surface, respectively. A dilation angle can also be defined, describing the change in volumetric strain associated with an increment in the shear strain. The volumetric response to hydrostatic pressure is linear and defined by the elastic shear modulus and Poisson's ratio values established by the user. The general range of apparent cohesion according to the type of soil is tabulated in Table 1. Also, the corresponding input data for the first numerical example of soil-pile interaction are shown in Table 2. However, this material model does not allow the SPH elements in LS-DYNA program.

### *3.2 MAT147: FHWA soil model*

This material model was developed by Lewis (2004) for the Federal Highways Administration (FHWA) of USA for application to road-base soils. This model consists of two tri-axial compression tests and a hydrostatic tension test. It was proposed to predict the dynamic performance of roadside safety structures embedded in the horizontal or sloping ground that are subjected to a vehicle impact. The twenty-four input parameters for analysis of LS-DYNA are necessary, but only twelve main input parameters for the FHWA soil model are shown in Table 3, including the density in the initial state, bulk and shear modulus, compaction curve and yield surface. Input data from the baseline material parameters given by the model developer of FHWA soil have been slightly modified. Especially, the elastic modulus E is assumed to be 18 MPa based on Yoshida's SPT test results (Yoshida *et al*. 1988). The stiffness parameters K and G have been also changed according to the range of dense sand that is well explained in the paper by Lee *et al*. (2014). It is known by Lewis (2004) that there is a gradual decrease in the shear strength after the peak from the direct shear test. Thus, the residual shear strength denoted by PHIRES as shown in Table 3 is assumed to be 80 % of the peak value. Since the Mohr-Coulomb failure criteria are used in this FHWA soli model, the parameters for cohesion and the angle of internal friction should be determined through direct shear testing or tri-axial compression tests (Lee *et al*. 2014). The detailed description about parameters in Table 4 has been precisely explained in the reference (Lee *et al*. 2014). This material model is implemented for SPH elements in LS-DYNA program.

Table 1 General range of apparent cohesion

| Types of soil | | Apparent cohesion $C_u$ (kPa) |
|---|---|---|
| Sand | Coarse | 30-50 |
| | Medium | 15-30 |
| | Fine or silt | 0-15 |
| Clay | Very stiff | 100-200 |
| | Medium stiff | 25-100 |

Table 2 Input data of Mohr-Coulomb model for undrained clay

| | | | |
|---|---|---|---|
| RO(t/mm$^3$)* | $1.8 \times 10^{-9}$ | PHI(rad) | 0.087 |
| GMOD(MPa) | 3.3599 | CVAL(MPa) | 0.05 |
| RNU | 0.49 | PSI(rad) | 0 |

*RO: Mass density (t/mm$^3$); GMOD: Elastic shear modulus (MPa); RNU: Poisson's ratio; PHI: Angle of friction (rad); CVAL: Cohesion value (shear strength at zero normal stress, MPa); PSI: Dilation angle (rad)

Table 3 Modified material parameters in FHWA soil model

| RO (kg/mm$^3$)* | NPLOT | SPGRAV | RHOWAT (kg/mm$^3$) | VN | K (MPa) |
|---|---|---|---|---|---|
| $2.35 \times 10^{-6}$ | 3 | 2.79 | $1.0 \times 10^{-6}$ | 1.1 | 11.766 |
| G (MPa) | PHIRES | INTRMX | MCONT | ECCEN | COH (GPa) |
| 7.06 | 0.9 | 10 | 0.034 | 0.7 | $6.2 \times 10^{-6}$ |

*RO : Mass density (kg/mm$^3$); NPLOT : Plotting options; SPGRAV : Specific Gravity of Soil used to get porosity; RHOWAT: Density of water in model units (kg/mm$^3$); VN: Viscoplasticity parameter (strain-rate enhanced strength); K: Bulk Modulus (MPa); G: Shear modulus (MPa) PHIRES : The minimum internal friction angle (residual shear strength, rad); INTRMX : Maximum number of plasticity iterations; MCONT: Moisture Content of Soil (determines amount of air voids); ECCEN: Eccentricity parameter for third invariant effects; COH: Cohesion Shear strength at zero confinement (MPa)

Table 4 General range of bulk and shear moduli for Poisson's ratio $\mu$=0.25

| Soil types | Modulus of elasticity *E* (MPa) | Bulk modulus *K* (MPa) | Shear modulus *G* (MPa) |
|---|---|---|---|
| Loose sand | 10.35-24.15 | 6.90-16.10 | 4.14-9.66 |
| Medium dense sand | 10.35-17.25 | 6.90-11.50 | 4.14-6.90 |
| Dense sand | 17.25-27.60 | 11.50-18.40 | 6.90-11.04 |
| Silty sand | 34.50-55.20 | 23.00-36.80 | 13.80-22.08 |
| Sand and gravel | 69.00-172.50 | 46.00-115.00 | 27.60-69.00 |

## 4. SPH element

Apart from the grid-based method, the analytical domain by the particle-based SPH (Lucy 1977, Gingold 1977) model is discretized with particles and approximate solution is solved at the particles. Since no meshes are required, shape functions are constructed from the particles. This method is efficient for large material distortion, moving boundaries, adaptive procedure, *etc*, but some disadvantages are also detected such as high CPU and memory in implicit/explicit analysis, difficult essential boundary condition treatment, compatibility at the interface

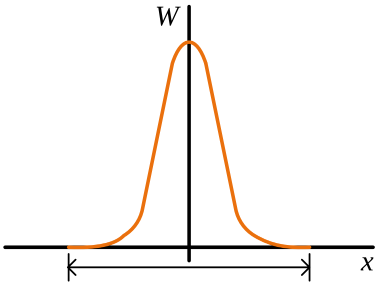


Fig. 3 Typical form of kernel function

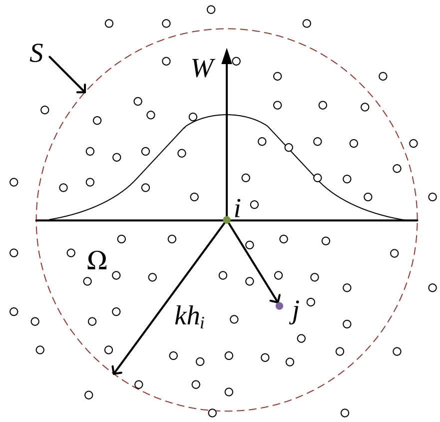


Fig. 4 SPH concept in the problem domain *Ω* with surface *S* (Liu 2010)

between solid and SPH elements. This method consists of two main steps such as domain discretization and numerical discretization. Domain discretization for the first step can be implemented by a set of arbitrarily distributed particles. In other words, derivatives at a particle using information at all the neighboring particles to approximate the values of functions. The field function $f$(x) can be defined in Eq. (7) using Dirac delta function $\delta$(x) that is a unit impulse symbol.

$$f(x) = \int_{\Omega} f(x')\delta(x - x')dx' \tag{7}$$

This function $\delta(x\text{-}x')$ is replaced by a smoothing function $W(x\text{-}x',h)$ that is called kernel function as well to interpolate particles within the support domain. Basic properties of smoothing function in SPH formulation are normalization condition (unity condition), delta function property and compact condition when the smoothing length $h \rightarrow 0$ as shown in Fig. 3 (Liu 2010).

$$f(x) = \int_{\Omega} f(x')W(x - x', h)dx' \tag{8}$$

Considering the local domain Ω, called support domain, filled with a set of particles in Fig. 4, the particle approximation with respect to displacement and its derivatives in Eqs. (9)-(12) are needed for numerical discretization for the second step. The volume of a subsection is lumped on the corresponding particle. One particle $i$ is associated with a fixed lumped volume $\Delta V_i$ in Eq. (9). If the particle mass and density are known, the lumped volume can also be replaced by the corresponding mass to density ratio denoted by $m_i/\rho_i$, in Eq. (10) where $N$ represents the total number of particles within the support domain.

$$f(x) \cong f(X) = \sum_{j=1}^{N} f(X_j)W(X - X_j, h)\Delta V_j$$
$$= \sum_{j=1}^{N} f(X_j)W(X - X_j, h)\frac{1}{\rho_j}(\rho_j \Delta V_j) \quad (9)$$
$$= \sum_{j=1}^{N} f(X_j)W(X - X_j, h)\frac{1}{\rho_j}(m_j)$$

$$\therefore f(X) = \sum_{j=1}^{N} \frac{m_j}{\rho_j} f(X_j)W(X - X_j, h) \quad (10)$$

Substituting $f(x)$ with $\nabla f(x)$ in Eq. (8) and integrating by parts, we obtain the derivative of the function by using the divergence theorem in Eqs. (11)-(12). Thus, the gradient is determined from the values of f and the derivatives of W, rather than from the derivatives of the function itself.

$$\nabla f(x) = \int_{\Omega} [\nabla f(x')]W(x - x', h)dx' \quad (11)$$

$$\nabla f(x) = \int_{\Omega} f(x')\nabla W(x - x', h)dx' \quad (12)$$

## 5. Numerical examples

### *5.1 Analysis of soil-pile interaction*

The lateral behavior of a single concrete pile has been tested as the first example to demonstrate the validity of present 3-D FE model since the numerical and theoretical solutions are available in literatures. The geometric configuration and material properties of undrained clay are those included in the reference data reported by Georgiadis and Georgiadis (2010, 2012) who used the linear elastic-perfectly plastic Tresca material model for soil afforded by the code Plaxis 3D Foundation V2.2. On the other hand, the MAT 173 (Mohr-Coulomb model) model available in LS-DYNA is adopted for soil modeling in this study since this model requires only six input soil data that can be obtained from above reference. However, this material model cannot be implemented for SPH element in LS-DYNA. Thus only the finite element model is fixed as illustrated in Fig. 5. In particular, two slope angles, $\theta = 0°$ and 30°, are considered for the horizontal and sloping grounds, respectively. The pile length, $L$ = 12 m, and pile diameter, $D$ = 1 m, are fixed. The circular shaped pile is assumed to be made of concrete material with elastic modulus, $E_p = 2.9 \times 10^7$ kPa. A typical 3-D finite element mesh consists of a six-node wedge form of pentahedral elements and eight-node hexahedral elements, as shown in Fig. 5. The main mechanical properties of the soil can be summarized as the undrained

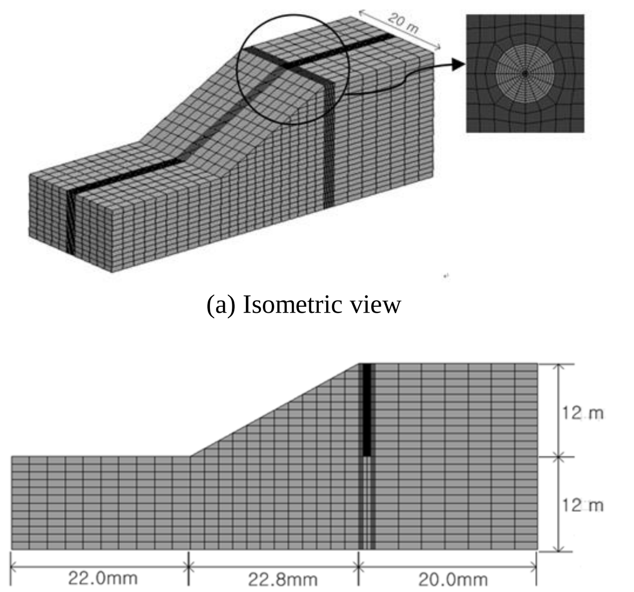


(a) Isometric view

(b) Front view

Fig. 5 Finite element modeling for sloping ground ($\theta$ = 30°)

shear strength of $C_u$ = 50 kPa, undrained Young's modulus of $E_s$ = 10 MPa, Poisson's ratio of $\nu$ = 0.49, and bulk unit weight of $\gamma$ = 18 kN/m$^3$. The boundaries along the bottom surface of FEM model are fixed in all directions and the degrees of freedom for vertical boundaries are fixed only in the normal direction. However, the top and inclined surfaces are not constrained. The horizontal load acting on the top of the circular concrete pile is considered as a uniform distribution load. To derive the theoretical solution from Eq. (2) to Eq. (5), necessary parameters are calculated by $N_{pu}$= 10.82, $N_{po}$ = 2.75 and $\lambda$ = 0.475. The initial stiffness of the $p$-$y$ curve is calculated as $K_i$ = 28.75 MPa by using Eq. (5).

The numerical results from the present model are shown in Figs. 6-8 to investigate the lateral response of single pile with respect to the ground inclination of 30°. The typical variation in lateral pile displacement $y$ along the pile length $z$ is presented with respect to load increment varying from 500 kN to 1500 kN as shown in Fig. 6. The increase in the lateral displacement may be attributed to lesser passive resistance available for sloping ground. Also, this increase becomes greater as the load level is increased. The shear force $Q$ along the pile is shown in Fig. 7. It is noted that the shear forces for $\theta$ = 30° are higher than those for the horizontal ground analysis at the top and lower part of the pile. The same tendency is detected, such that the shear forces become greater as the lateral load is increased. The numerical results obtained by the 3-D Mohr-Coulomb model are compared with the theoretical solution in Eq. (2) as well as the finite element solution afforded by the code Plaxis 3D Foundation V2.2. Georgiadis and Georgiadis (2010) used a linear elastic-perfectly plastic Tresca material model for soil. Even though same 3-D FEM models are used, numerical solutions are slightly different due to input data related to soil parameters, failure criteria, types of

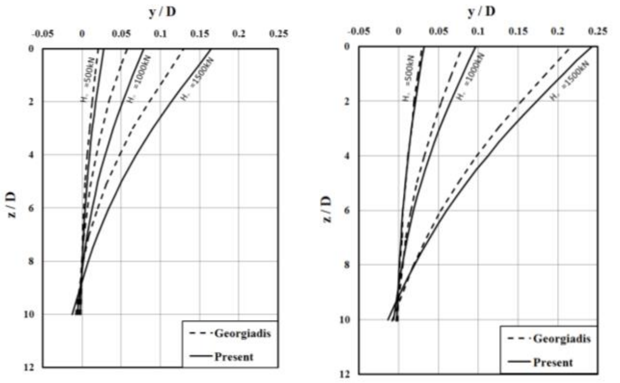


(a)Horizontal Ground ($\theta$ = 0°) (b)Sloping Ground ($\theta$ = 30°)

Fig. 6 Lateral displacement versus depth relationships from ground level

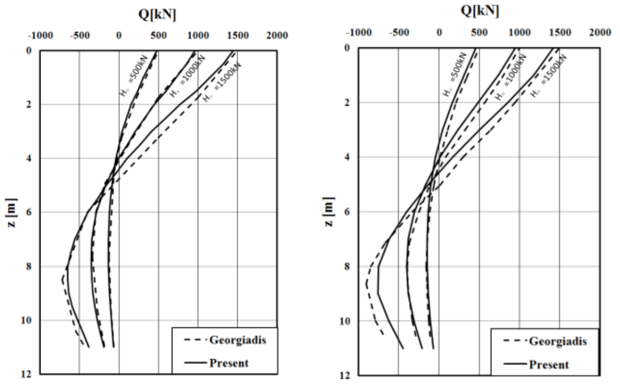


(a) Horizontal ground($\theta$ = 0°) (b) Sloping ground ($\theta$ = 30°)

Fig. 7 Lateral shear force versus depth relationships from ground level

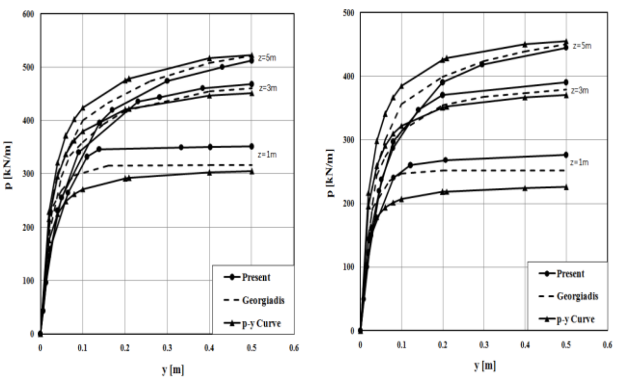


(a)Horizontal ground ($\theta$ = 0°) (b)Sloping ground ($\theta$ = 30°)

Fig. 8 Comparison of *p-y* curves along the depth

element consisting FEM model, algorithm for non-linear analysis and handling of interface constraint between soil and pile. Thus, a difference in the maximum lateral displacement is detected as the pile head load is increased, as shown in Fig. 6, which is mainly attributed to the soil parameters since the detailed soil properties are not presented in the reference (Georgiadis and Georgiadis 2012).

The variation of the shear force ($Q$) along the pile depth ($z$) as shown in Figs. 7-8 has been differentiated to estimate the soli pressure ($p$) as a function of the pile depth ($z$) as the pile head load $H_0$ is increased. The relationship between the shear force ($Q$) and soil reaction ($p$) is expressed by Eqs. (13)-(14).

$$Q = E_p I_p \frac{d^3 y}{dz^3} \tag{13}$$

$$p = E_p I_p \frac{d^4 y}{dz^4} \tag{14}$$

To derive *p-y* curve, firstly, the *Q-z* curve should be determined by the least square approach from the data of lateral displacements at the selected points of pile length. In this study, the *Q-z* curve is assumed to be fifth-order polynomials by a suitable curve fitting procedure available in EXCEL program. Secondly, this curve determines the most appropriate equation for a given set of data and provides the *p-z* curve that is the first derivative of the *Q-z* diagram. Thirdly, the *p-z* diagrams can be derived in combination with the *y-z* diagrams in Fig. 6. The corresponding *p-y* curves obtained by the present 3-D FE model, which are illustrated in Fig. 8, model have been compared with the theoretical solutions given by Eq. (2) and numerical analyses performed by Georgiadis and Georgiadis (2010, 2012) for the horizontal and the sloping ground, respectively.

It is noted that the maximum lateral displacements for the horizontal ground are 0.0268 m, 0.0781 m, and 0.171 m when the pile head loads $H_0$ are 500 kN, 1000 kN, and 1500 kN, respectively. On the other hand, 0.032, 0.0961, and 0.244 m for sloping ground. The decrease in the passive resistance of single pile due to the ground inclination is significantly pronounced. It is known that when the inclination angle is 30°, the passive resistance of the sloping ground shows an approximately 30 % decrease as compared with that of the horizontal ground. Also, Figs. 8-9 show the contours of the von-Mises stress when the pile head loads $H_0$ are 500 kN, 1000 kN and 1500 kN, respectively. As expected, the maximum stress zones spread out as the lateral load is increased.

### *5.2 Analysis of soil-guardrail post interaction*

In this example, the hybrid model combining 3-D finite elements with SPH elements in the vicinity of a guardrail post is shown in Fig. 11 to estimate the lateral resistance of the guardrail post in order to compare it with the numerical results obtained by only 3-D FE model. The material model for the soil is based on FHWA soil (MAT 147) in LS-DYNA that was developed by the Federal Highway Administration of the USA for applications involving road-base soils. The standard soil tests for determining the mechanical properties, developed by Kulak and Schwer (2012), include the hydrostatic compression and trial compression tests that are performed by causing all three principal stresses to be the same, as shown in Tables 3-4. On the other hand, a steel post embedded 1500 mm into the ground is modeled by four-node Belytschko-Tsayshell elements with three integration points and the piecewise-linear-plasticity model (MAT 24) available in LS-DYNA. A cross section of the steel post is considered with a width of $D$ = 125 mm and thickness of 4 mm. Table 4 lists the input parameters used

Table 5 Input data of piecewise linear plasticity model for steel post

| | |
|---|---|
| Density (t/mm$^3$) | $7.85 \times 10^{-9}$ |
| Elastic Modulus (MPa) | $2.1 \times 10^5$ |
| Poisson's Ratio | 0.3 |
| Yield Stress (MPa) | 250 |

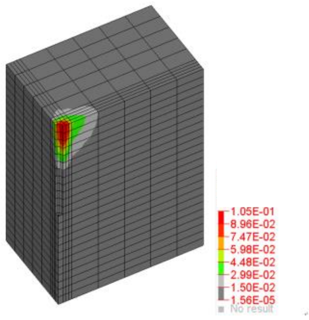


(a) 500kN

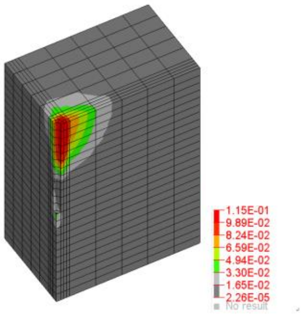


(b) 1000kN

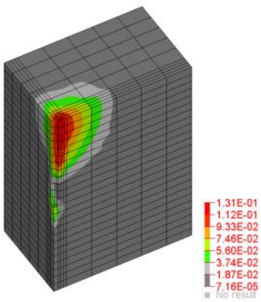


(c) 1500kN

Fig. 9 Distribution of von-Mises stress for horizontal ground

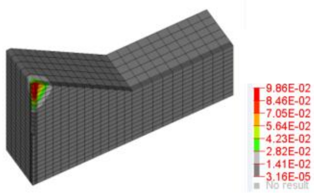


(a) 500kN

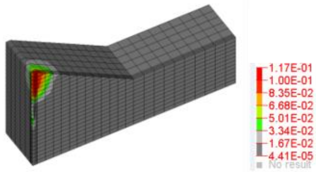


(b) 1000kN

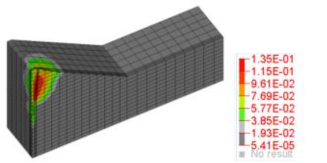


(c) 1500kN

Fig. 10 Distribution of von-Mises stress for sloping ground

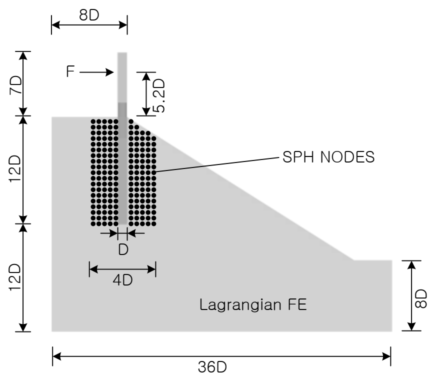


Fig. 11 Problem definition of a laterally loaded guardrail post in sloping ground

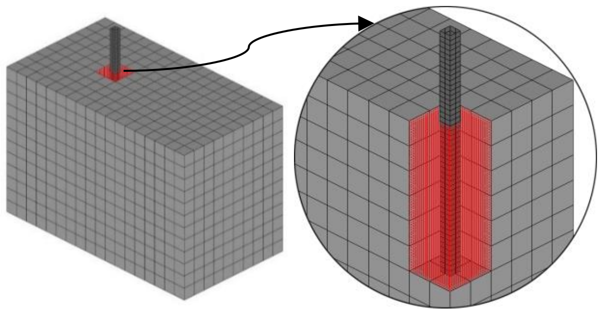

Fig. 12 SPH model of single guardrail post in horizontal ground for SPH pitch = 25 mm

to define the steel materials.

The schematic diagram in Fig. 12 shows a laterally loaded post embedded in 1 : 1.5 ($\theta$ = 30°) sloping ground. The boundary conditions are exactly same as the example in the previous section. The horizontal load $F$ is applied at 5.2$D$ (650 mm) from the ground level, as shown in Fig. 11. The quasi static loading is considered in explicit simulations with a loading rate of 100 mm/sec and lateral displacements of up to 500 mm for 5 seconds. The rigid cover plate attached to the steel post at the loading point is controlled by increasing the displacement at a given loading rate.

To define the general control parameters including initial smoothing length, part ID, material law and mass of the particle, *CONTROL_SPH, *SECTION_SPH, and *ELEMENT_SPH have been used. A flag is activated to show the presence of SPH particles during SPH calculation. The contact between the soil and single guardrail post is modeled with a suitable CONTACT option, such as

CONTACT_AUTOMATIC_SURFACE_TO_SURFACE. The interaction between the soil and guardrail post is also modeled through the CONSTRAINED_LAGRANGE_IN_ SOILD optional card. The region of soil experiencing large deformations in the vicinity of the guardrail post is modeled by SPH particles, as shown in Fig. 11. The size of the SPH zone is four times the diameter of the post $D$ in the vicinity of the post. The rest of the model further away from the highly distorted soil is based on the conventional Lagrangian 3-D elements. The SPH particles at the Lagrange element interface are tied to the Lagrangian portion of the soil material using the CONTACT_TIED_NODES_TO_SURFACE command (Borovinsek *et al*. 2007). The detailed numerical models consisting of the conventional Lagrangian 3-D elements and SPH elements are illustrated in Figs. 12-13 for the horizontal ground and sloping ground. In this study, three different pitches (or particle spacing) for the SPH model of 12.5, 25, and 50 mm are used to check the convergence of the solution. Based on the convergence test, the SPH pitch is fixed at 25 mm. The numbers of SPH and 3-D FE elements are 26,901 and 2,136 in Fig. 12, and 25,620 and 24,800 in Fig. 13, respectively.

The lateral displacements of the guardrail post at the loading point are computed for horizontal ground as well as for sloping ground. In the case of horizontal ground, the maximum lateral resistances of the post determined by SPH analysis and 3-D FE analysis are 45.4 kN and 51.7 kN, respectively, as shown in Fig. 14. On the other hand, the maximum lateral resistances for sloping ground are found to be 41.0 kN and 45.3 kN by 3-D FE analysis, respectively, as compared with the value of 40 kN obtained by the experimental field test at KECRI (Korea Expressway Corporation Research Institute) that is the main test facility for testing road equipment in Korea, as shown in Fig. 15.

It is noted that the SPH results for a pitch of 25 mm yield a lower lateral resistance than that obtained by the 3-D FE method. This may be attributed to the large distortion effect of the soil meshes when the conventional 3-D Lagrangian finite element approach is used. It may be noted that the maximum lateral resistance of the guardrail post is reduced by approximately 12% based on the FEM results, due to the effect of the ground inclination. Also, the flexural failure of the guardrail post is more significant than the shear failure of the soil, since the horizontal load F applied at 5.2$D$ (650 mm) from the ground level induces a bending moment about the ground surface. In the case of the pile-soil interaction in previous section, however, the passive resistance for the sloping ground showed an approximately 30% decrease as compared with the horizontal ground condition. This means that the shear failure of the soil is dominant for the soil-pile interaction, since the massive concrete pile with a diameter of $D$ = 1.0 m and length $L$ = 12 m is totally embedded into the ground that is subjected to the lateral load at the pile head.

The variation of the lateral displacements of a single guardrail post is plotted with respect to embedment depth from the ground level in Figs. 16-17 when the lateral load $F$ is fixed at 40 kN. Generally, as displacements are converged with reduction of particle spacing, convergence tests are implemented from 37.5 mm to 12.5 mm at interval of

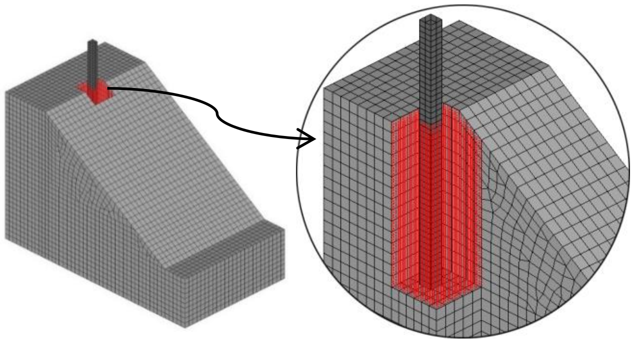

Fig. 13 SPH model of single guardrail post in sloping ground for SPH pitch = 25 mm

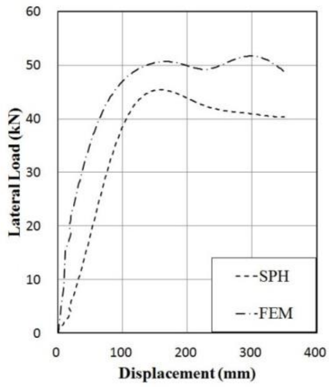


Fig. 14 Load-displacement relation for horizontal case

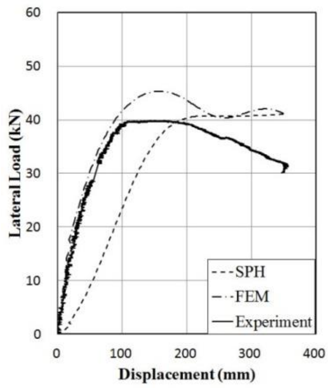


Fig. 15 Load-displacement relation for sloping case

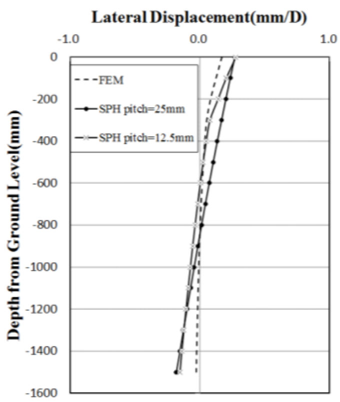


Fig. 16 Lateral displacement from the ground level in the horizontal case ($F$ = 40 kN)

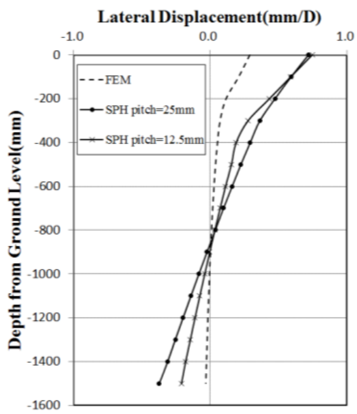


Fig. 17 Lateral displacement from the ground level in the sloping case ($F$ = 40 kN)

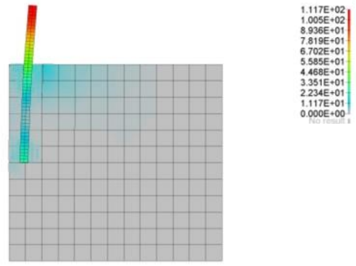

(a) $F$ = 20 kN

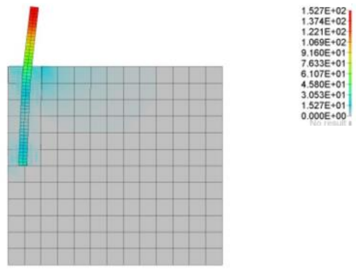

(b) $F$ = 30 kN

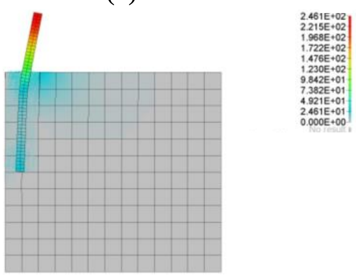

(c) $F$ = 40 kN

Fig. 18 Displacement variations for the horizontal cases

6.25mm. As representative cases, two results considering the particle spacing of 25 and 12.5 mm respectively are plotted in Figs. 16 and 17. It is seen that the displacements of SPH are closer to those of FEM with reduction of the particle spacing. Also, the lateral displacements at the ground surface obtained using the 3-D FE analysis are computed to be 21 mm and 36 mm for the horizontal and sloping cases, respectively. The lateral displacements obtained using the SPH model are found to be 34 mm and 69 mm for the horizontal and sloping cases, respectively. It is noted that the stiffness of the artificial soil in the case of

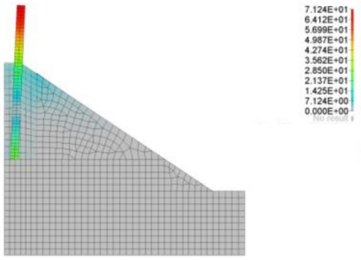

(a) $F$ = 20 kN

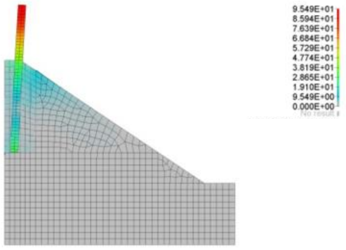

(b) $F$ = 30 kN

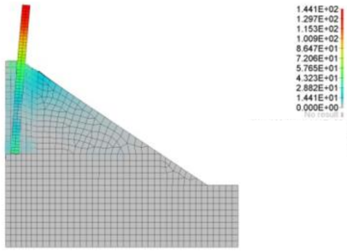

(c) $F$ = 40 kN

Fig. 19 Displacement variations for the sloping cases

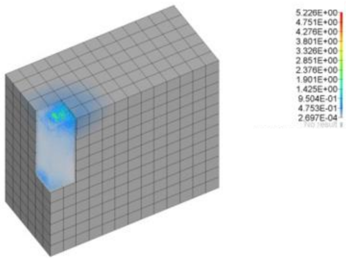

(a) $F$ = 20 kN

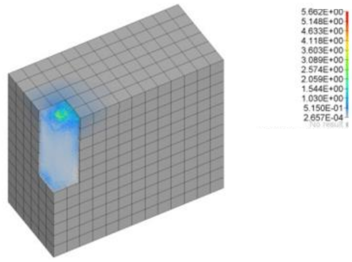

(b) $F$ = 30 kN

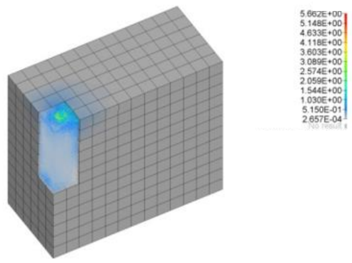

(c) $F$ = 40 kN

Fig. 20 von-Mises stress distribution for horizontal cases

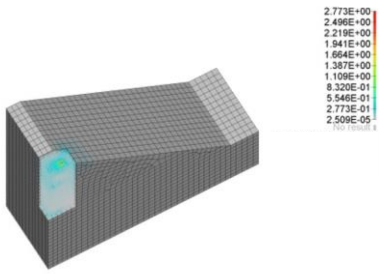

(a) $F$ = 20 kN

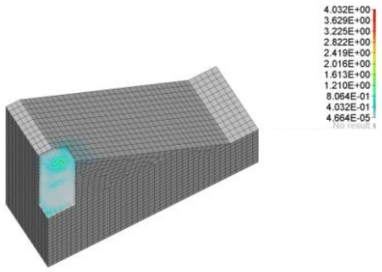

(b) $F$ = 30 kN

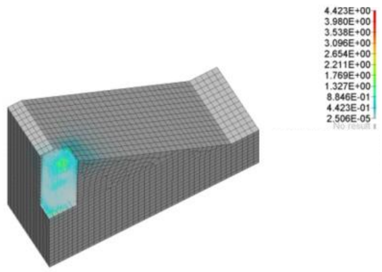

(c) $F$ = 40 kN

Fig. 21 von-Mises stress distribution for sloping cases

the 3-D Lagrangian finite element model may be overestimated, due to the increasing distortion effect of the soil meshes as the lateral movement of the guardrail post becomes large. This tendency agrees with the analysis of the lateral resistance due to the softening effect of the SPH approach. Also, the variation of the lateral displacement in both cases is graphically shown in Figs. 18 and 19 as the load level is increased from 20 kN to 40 kN. Figs. 20 and 21 show the contours of the von-Mises stress when the lateral loads F are 20 kN, 30 kN and 40 kN. As expected, the maximum stress zones spread out as the lateral load is increased.

## 6. Conclusions

The main purpose of this paper is to demonstrate the application of 3-D finite element model as well as SPH model for the evaluation of the lateral resistance of a single concrete pile or single guardrail post placed near slopes. The conclusions from this study can be derived as follows:

(1) The lateral resistance of the single pile decreases as its location approaches the crest of the slope. It may be concluded that the passive resistance for the sloping ground shows an approximately 30% decrease as compared with the horizontal ground condition when the ground slope is 1 : 1.5 ($\theta$ = 30°). In this case, the shear failure of the soil is dominant, since the concrete pile with a diameter of $D$ = 1.0 m and length $L$ = 12 m is totally embedded into the ground that is subjected to the lateral load at the pile head. However, the maximum lateral resistance of the guardrail post obtained from the load-displacement curve in Figs. 14-15 is reduced by approximately 12%, due to the effect of the ground inclination. In the case of the soil-post interaction, the flexural failure of the guardrail post is more profound than the shear failure of the soil, since the horizontal load $F$ applied at 5.2$D$ (650 mm) from the ground level causes a bending moment about the ground surface.

(2) In agreement with both the empirical solution and FE analysis using Plaxis 3D Foundation V2.2, the proposed soil material model shows the proper *p-y* curves. The load-pile head displacement relationships are predicted with remarkable agreement for the single pile test under lateral soil movement.

(3) It is noted that the hybrid model consisting of 3-D finite elements and SPH elements gives a lower lateral resistance than the results obtained by 3-D FE analysis only. This may be attributed to the large distortion effect of the soil meshes when only the conventional 3-D Lagrangian finite element approach is adopted.

## Acknowledgements

This research was supported by Basic Science Research Program through the National Research Foundation of Korea(NRF) funded by the Ministry of Education(NRF-2016R1D1A1A09919557).

## References

Borovinsek, M., Vesenjak, M., Ulbin, M. and Ren, Z. (2007), "Simulation of crash tests for high containment levels of road safety barriers", *Eng. Fail. Anal.*, **14**(8), 1711-1718.

Cabalar, A.F. (2016), "Cyclic behavior of various sands and structural materials interfaces", *Geomech. Eng.*, **10**(1), 1-19.

Carter, D.P. (1984), "A non-linear soil model for predicting lateral response", Ph.D. Dissertation, University of Auckland, Auckland, New Zealand.

Chae, K.S., Ugai, K. and Wakai, A. (2004), "Lateral resistance of short single piles and pile groups located near slopes", *J. Geomech.*, **4**(2), 93-103.

Georgiadis, K. and Georgiadis, M. (2010), "Undrained lateral pile response in sloping ground" *J. Geotech. Geoenviron. Eng.*, **136**(11), 1489-1500.

Georgiadis, K. and Georgiadis, M. (2012), "Development of p-y curves for undrained response of piles near slopes", *Comput. Geotech.*, **40**, 53-61.

Gingold, R.A. and Monaghan, J.J. (1977), "Smoothed particle hydrodynamics-theory and application to non-spherical stars", *Mon. Not. R. Astron. Soc.*, **181**(3), 375-389.

Hirai, H. (2012), "A Winkler model approach for vertically and laterally loaded piles in nonhomogeneous soil", *J. Numer. Anal. Meth. Geomech.*, **36**(17), 1869-1897.

Jafarnia, M. and Varzaghani, M.I. (2016), "Effect of near field earthquake on the monuments adjacent to underground tunnels using hybrid FEA-ANN technique", *Geomech. Eng.*, **10**(4), 757-768.

Jiang, H. and Xie, Y. (2011) "A note on the Mohr-Coulomb and Drucker-Prager strength criteria", *Mech. Res. Commun.*, **38**(4), 309-314.

Kim, B.T., Kim, N., Lee. W.J. and Kim, Y.S. (2004), "Experimental load-transfer curves of laterally loaded piles in Nak-Dong River sand", *J. Geotech. Geoenviron. Eng.*, **130**(4), 416-425.

Kulak, R.F. and Schwer, L. (2012), "Effect of soil material models on SPH simulations for soil-structure interaction", *Proceedings of the 12th International LS-DYNA Users Conference*, Dearbon, Michigan, U.S.A, June.

Lee, D.W., Ahn, J.S., and Woo, K.S. (2014), "Vehicle impact analysis of flexible barriers supported by different shaped posts in sloping ground", *Adv. Mech. Eng.*, **6**, 1-8.

Lewis, B.A. (2004), *Manual for LS-DYNA Soil Material Model 147*, FHWA-HRT-04-095, APTEK, Incorporated, Colorado Springs, Colorado, U.S.A.

Lingenfelter, J.L., Rosenbaugh, S.K., Bielenberg, R.W., Lechtenberg, K.A., Faller, R.K. and Reid, J.D. (2016), *Midwest Guararail System(MGS) with an Omitted Post*, Report No. TRP-03-326-16.

Liu, M.B. and Liu, G.R. (2010), "Smoothed particle hydrodynamics(SPH): An overview and recent developments", *Arch. Comput. Meth. Eng.*, **17**(1), 25-76.

LSTC (2012), *LS-DYNA Keyword User's Manual*, (Version 971 R6.0.0), Livermore Software Technology Corporation, Livermore, California, U.S.A.

Lucy, L.B. (1977), "A numerical approach of the testing of the fission hypothesis", *Mon. Not. R. Astron. Soc.*, **82**(12), 1013-1024.

Matlock, H. (1970), "Correlation for design of laterally loaded piles in soft clays", *Proceedings of the 2nd Offshore Technology Conference*, Houston, Texas, U.S.A., May.

Murff, J.D. and Hamilton, J.M. (1993), "P-ultimate for undrained analysis of laterally loaded piles", *J. Geotech. Eng.*, **119**(1), 91-107.

Nastasescu, V. (2010), "SPH method in applied mechanics", *UPB Sci. Bull. Ser. D Mech. Eng.*, **72**(4), 13-20.

Plaxico, C., Patzner, G. and Malcom, R. (1998), "Finite element modeling of guardrail timber posts and post-soil interaction", *Transport. Res. Record J.*, (1647), 139-146.

Reese, L.C., Cox, W.R. and Koop, F.D. (1974), "Analysis of laterally loaded piles in sand", *Proceeding of the 6th Offshore Technology Conference*, Houston, Texas, U.S.A., May

Reese, L.C. and Welch, R.C. (1975), "Lateral loading of deep foundations in stiff clay", *J. Geotech. Eng.*, **101**(7), 633-649.

Sheikh, N.M., Abu-Odeh, A.Y. and Bligh, R.P. (2011), "Finite element modeling and validation of guardrail steel post deflecting in soil at varying embedment depths", *Proceeding of the 11th International LS-DYNA Users Conference*, Dearbon, Michigan, U.S.A., June.

Sheikh, N.M., Bligh, R.P. and Menges, W.L. (2009), *Guidelines for W-beam Guardrail Post Installation in Rock,* Report No. 405160-7-1, Texas Transportation Institute, Texas, U.S.A.

Vesic, A.S. (1961), "Beam on elastic subgrade and the Winkler hypothesis", *Proceedings of the 5th International Conference for Soil Mechanics*, Paris, France, July.

Wu, W. and Thomson, R. (2007), "A study of the interaction between a guardrail post and soil during quasi-static and dynamic loading", *J. Impact Eng.*, **34**(5), 883-898.

Yoshida, Y., Motonori, I. and Kokusho, T. (1988), "Empirical formulas of SPT blow-counts for gravelly soils", *Proceedings of the 1st International Symposium on Penetration Testing*, Orlando, Florida, U.S.A., March.

Zhang, C., Ji, J., Gui, Y., Kodikara, J., Yang, S. and He, L. (2016), "Evaluation of soil-concrete interface shear strength based on LS-SVM", *Geomech. Eng.*, **11**(3), 361-372

*JS*